Image acceleration of highly charged ions by metal surfaces

C. Lemell, H. P. Winter, and F. Aumayr
Institut für Allgemeine Physik, TU Wien, 1040 Wien, Austria

J. Burgdörfer and F. Meyer
Department of Physics, University of Tennessee, Knoxville, Tennessee 37996-1200,
Oak Ridge National Laboratory, Oak Ridge, Tennessee 37831-6377
(Received 5 September 1995)

We present classical simulations for the energy gain, ΔE, due to the image acceleration of very highly charged ions ($Q \gg 10$) by metal surfaces. We show that for large Q the simulated values ΔE, based on the classical over-barrier model, fall below the "staircase" model but still exceed the lower bound for classically allowed transitions. The results are in reasonable agreement with recent experimental data. Effects of the nonzero velocity of the projectile parallel to the surface appear to be insignificant for the energy gain.

PACS number(s): 34.50.Dy

I. INTRODUCTION

A highly charged ion with charge $Q \gg 1$ approaching a metallic surface polarizes the conduction band and, thereby, experiences an attractive force. In terms of image charges of classical electrostatics this force along the surface normal is given by

$$F_z = -Q^2/4R^2, \tag{1}$$

where R is the distance of the ion from the surface. For highly charged ions, the resulting acceleration leads to a sizable energy gain, ΔE, of the ions approaching the surface at low velocities ($v_z \lesssim 10^{-2}$ a.u.). As the initial charge $Q = Q_i$ rapidly changes as a result of multiple electron capture and loss processes, the resulting energy gain ΔE becomes a sensitive measure for where and how quickly a highly charged ion is neutralized, i.e., where a hollow atom is formed above the surface.

Recently, measurements for ΔE have been performed in the grazing incidence geometry ($v_\parallel \lesssim 0.4$ a.u., $v_\perp < 10^{-2}$ a.u.) for charge states up to 36 [1–3] while in the normal incidence geometry ΔE has been measured up to $Q = 79$ yielding energy gains up to $\simeq 780$ eV [4]. While the former measurements are based on the detection of the angular deflection of the specularly reflected beam due to the image field, the latter employs the saturation of the electron-emission yields as a function of the deceleration voltage. All sets of data appear to follow the trend of the previously proposed "staircase" model of sequential neutralization [5] which represents a simplified analytical treatment of the classical over-barrier (COB) model [6]. Another simplified version of the COB model relies on a Q-independent transition rate [7]. However, the data taken at grazing incidence [2,3], which are more accurate, appear to lie systematically below the predictions of the staircase model for charge states $Q \gtrsim 30$. This observation gave rise to speculations as to possible saturation effects which could be indicative of either the modifications of the dielectric response of a surface in the presence of extremely strong Coulomb field or of parallel-velocity effects.

In this paper we investigate the energy gain due to image acceleration for very high charge states using the full simulation code for the classical over-barrier dynamics [6]. We analyze the validity of the COB model for very high charge states and discuss possible effects of nonvanishing parallel velocities. We find that the results of the simulation for higher charge states fall, indeed, below that of the staircase model in contrast to previously investigated lower charge states [5] where the energy gain exceeded that of the staircase model. The crossover occurs around $Q \simeq 15$. Our results are, within the limitations of the experimental uncertainty and the limitations of the model, in good agreement with experiments.

II. VALIDITY OF THE COB MODEL FOR LARGE Q

In our simulation we employ the COB model, which has been described in Ref. [6] and to which we refer the reader for further details. We focus here on a few aspects which deserve scrutiny as to their validity in the limit of $Q \to \infty$.

Electrons near the Fermi edge of metal surfaces, represented by a nearly free electron gas, can be effectively transferred resonantly to the incident projectile when the potential barrier between the metal and the projectile drops below the Fermi level, i.e, when the transfer becomes classically allowed. Classical over-barrier transitions set in at a distance from the surface

$$R_c(Q) \simeq \sqrt{8Q+2}/2W \simeq \sqrt{2Q}/W \tag{2}$$

(W is the work functions of the metal). As $Q \gg 1$, capture takes place into increasingly higher n shells and the validity of the classical model should improve. Equation (2) is derived using classical image potentials. For more realistic potentials (see below), R_c increases slightly but Eq. (2) remains a good first-order estimate. The simplified analytical staircase model follows now from Eq. (2) with the help of two additional assumptions: (a) the charge transfer occurs instantaneously as soon as it is classically allowed and (b) the

captured electron screens one unit charge of the projectile completely. Consequently, the effective charge will be reduced to $Q-1$ at the distance $R_c(Q)$ and will be constant until the next critical distance $R_c(Q-1)$ is reached. The energy gain along the staircase sequence of stepwise neutralization is given by

$$\Delta E = \frac{W}{2} \sum_{i=0}^{Q-1} \frac{2(Q-i)-1}{\sqrt{8(Q-i)}}. \tag{3}$$

In the limit of large Q, the sum in (3) can be converted to an integral, yielding the asymptotic expansion in Q,

$$\Delta E = \frac{W}{2\sqrt{2}}[\tfrac{2}{3}Q^{3/2} - \tfrac{3}{4}Q^{1/2} + 0.521] + O(Q^{-1/2}). \tag{4}$$

Equations (3) and (4) predict a linear scaling of the energy gain with the work function, i.e., $\Delta E/W$ should be a universal function for all metal surfaces. Furthermore, $\Delta E/W$ should scale as $Q^{3/2}$ as $Q \to \infty$. The validity of these assumptions, analyzed so far [5] only for multiply charged ions ($Q \leqslant 8$), will be tested in the following for highly charged ions.

The saddle point of the potential barrier and, hence, Eqs. (2) and (3) are based on the classical image limit of the effective interaction potential near the surface,

$$V(\vec{r},\vec{R}) = V_p(Q,\vec{r}-\vec{R}) + V_p^I(Q,R) + V_{pe}^I(Q,\vec{r},\vec{R}) + V_e^{SI}(\vec{r}), \tag{5}$$

where V_p is the direct (and, in general, screened) Coulomb interaction between the active electron and the projectile and V_e^{SI} describes the electronic interaction with the jellium surface. In the simulation we use a numerical fit to the model potential proposed by Jenning, Jones, and Weinert [8]. It reproduces the self-consistent local-density approximation (LDA) calculation of Kohn and Lang [9] near and inside the surface (apart from the Friedel oscillations) while giving the correct asymptotic behavior $\sim -1/4(z-d)$, where d denotes the displacement of the image plane relative to the surface (taken to be a jellium surface in the following). The potentials V_p^I and V_{pe}^I describe the interaction of the projectile with its own image which is responsible for the image acceleration [see Eq. (1)] and the interaction of the electron with the projectile image, respectively.

The linear Q dependence of the dynamical screening potentials relies on the validity of the linear-response theory. In the limit of small perpendicular velocities ($v_z \to 0$) we have for the interaction between the electron and the projectile image [10]

$$V_{pe}^I(Q,\vec{\rho},z,R) = -Q \int_0^\infty dk\ J_0(k\rho) e^{-k[|z|+(R-2d)]} \times \frac{1-\epsilon_s(k,v_\parallel k)}{1+\epsilon_s(k,v_\parallel k)}, \tag{6}$$

where $\epsilon_s(k,\omega)$ is the surface dielectric function and $(\vec{\rho},z)$ are the cylindrical coordinates of the electron. For $\epsilon_s(k,\omega)$ we use the plasmon-pole approximation. Likewise, the interaction V_p^I follows from the expression (6) as $V_p^I = -QV_{pe}^I(\rho=0,z=r,R)/2$. In Eq. (6) we have displaced the ionic image plane by the distance d such that the specular reflection model (SRM) [10–12] underlying (6) yields the correct behavior of the image potential to order R^{-2} as $R \to \infty$. We note, however, that this correction becomes increasingly unimportant as $Q \to \infty$. The relevant region of R for which V_{pe}^I is evaluated is given by Eq. (2). Therefore

$$d/R \simeq d/R_c \underset{Q\to\infty}{\to} 1/\sqrt{Q}. \tag{7}$$

Validity of the linear-response theory requires the maximum induced surface charge density, $\delta\sigma \simeq Q/2\pi R^2$, to remain small compared to the charge density of the metal surface (jellium), $\sigma \simeq k_F^2/3\pi^2$ (k_F is the Fermi wave number) [13]. At a critical distance R_c [Eq. (2)] where the charge of the projectile is reduced by electron capture, the induced charge density is

$$\delta\sigma \simeq \frac{W^2}{4\pi}. \tag{8}$$

The remarkable observation is therefore that the induced charge density is effectively independent of Q at the point R_c and the validity of linear response hinges only on the fact that

$$\delta\sigma/\sigma = \frac{3}{4}\frac{\pi W^2}{k_F^2} \ll 1, \tag{9}$$

which is well satisfied for typical values of W and k_F for metals. For the determination of the critical distance R_c entering Eq. (8), the validity of the asymptotic image limit of (6) was assumed. This limit can be derived by expanding the surface response function for small k [9,10],

$$\frac{1-\epsilon_s(k,v_\parallel k)}{1+\epsilon_s(k,v_\parallel k)} = -1 + \frac{\alpha k}{\omega_s^2} + O(k^2), \tag{10}$$

where $\alpha = \sqrt{\tfrac{3}{10}}k_F\omega_p$ and $\omega_s = \omega_p/\sqrt{2}$ is the surface plasmon frequency (ω_p is the bulk plasmon frequency). Upon insertion of Eq. (10) into Eq. (6), the first term in Eq. (10) yields the classical image limit, $Q/2(z+R-2d)$, while the leading correction is of the order of

$$\frac{Q}{R_c}\left\langle \frac{\alpha k}{\omega_s^2} \right\rangle \simeq \frac{Q}{R_c^2}\frac{\alpha}{\omega_s^2} \simeq \frac{\alpha W^2}{\omega_p^2} \ll 1, \tag{11}$$

which is, again, independent of Q. We note that the term linear in k in Eq. (10) model determines the position of the image plane within the SRM, unless the displacement is explicitly incorporated, as has been done in Eq. (6). In Eq. (11) we made use of the fact that the range of k effectively sampled in the integral [Eq. (6)] is delineated by $k \lesssim R_c^{-1}(Q)$. The correction terms become therefore increasingly unimportant as $Q \to \infty$. We also note that the parallel velocity dependence of the potential [Eq. (6)] which is of the

order k^2 can be neglected for the same reason.

Effects of the parallel velocity $v_\parallel$ of the projectile on the charge transfer can be taken into account within the COB model. To this end, the spectral density $D(\epsilon)$, as seen in the projectile frame, is described by a Galilei shifted Fermi sphere [14–16].

$$D(\epsilon)=\frac{1}{\pi^2}\times\begin{cases}\sqrt{2\epsilon}, & \epsilon<\frac{1}{2}(v_F-v_\parallel)^2\\ \frac{1}{2}\sqrt{2\epsilon}+\dfrac{(v_F^2-v_\parallel^2)/2-\epsilon}{v_\parallel}, & \frac{1}{2}(v_F-v_\parallel)^2\leqslant\epsilon\leqslant\frac{1}{2}(v_F+v_\parallel)^2\\ 0, & \epsilon>\frac{1}{2}(v_F+v_\parallel)^2,\end{cases}\tag{12}$$

where we have assumed $v_\parallel<v_F$. The Galilei transformed spectral density is, however, not isotropic and only the component of the kinetic energy along the surface normal determines the effective flux of electrons across the barrier. The latter is, however, unaffected by the Galilei transform. Parallel-velocity effects could enter into the above-surface neutralization through elastic Coulomb scattering at the projectile which can redirect the electron gas moving, on the average, with velocity $-v_\parallel$, as seen in the projectile frame. The force F_z exerted by the passing-by projectile can be estimated for the classical image potential as

$$F_z\simeq\frac{2QR}{[R^2+(v_\parallel t)^2]^{3/2}}.\tag{13}$$

The resulting change in velocity follows from

$$\Delta v_z=F_z\Delta t\simeq F_z\frac{z_s}{v_z},\tag{14}$$

where z_s is the position of the saddle,

$$z_s=\frac{R}{\sqrt{2Q+8}},\tag{15}$$

and v_z is the velocity along the surface normal and is of the order v_F. Therefore,

$$\Delta v_z\simeq\frac{2Q}{R_c v_z\sqrt{2Q+8}}\simeq\frac{1}{2}\frac{W}{v_F}\simeq v_F\left(\frac{W}{4\epsilon_F}\right).\tag{16}$$

The normal component of momentum transfer is therefore also independent of Q for over-barrier transitions. Furthermore, the momentum transfer is small for typical metals and is not expected to yield a significant fraction of the electrons with energies along the surface normal exceeding the Fermi energy. Note that the estimate [Eq. (16)] would break down for very small $v_z\ll v_F$. However, solving the equation of motion [Eq. (13)] for this case yields the same conclusions for large R_c as long as $R_c\gg v_\parallel\Delta t$. Parallel-velocity effects are therefore unlikely to be important for above-surface charge transfer at large distances from the surface. They are, however, important for neutralization processes at and below the surface [17–20].

For very high projectile charge states $Q\gg1$, the maintenance of the quasineutrality of the ''hollow atom'' above the surface requires a relatively high electron density extending from the surface to distances well beyond the distance R of the projectile core from the surface. It is therefore tempting to visualize the charge cloud of the hollow atom as an extension of the conduction band into the vacuum. However, even for very high Q the electronic density of the hollow atom, ρ_A, remains small compared to the electronic density in the bulk, ρ_b. Assuming the charge cloud of the hollow atom to be confined to a sphere of radius R equal to the distance from the surface, we find for the density ratio

$$\rho_A/\rho_b\simeq Q^{1/3}(r_s/R),\tag{17}$$

where r_s is the Wigner-Seitz radius of the metal. Even for $Q\simeq40$, where the hollow atom formation begins at $R\simeq45$ a.u., the shrinking charge cloud reaches metallic densities only for $R\leqslant10$. In fact, our simulation yields considerably smaller ratios ρ_A/ρ_b than estimated by Eq. (17) since the charge cloud extends on the vacuum side considerably further than R.

III. SIMULATION RESULTS

We have performed a large number of simulations of the energy gain using the previous COB simulation code [6]. It should be stressed from the outset that in the light of the complexity of the multielectron processes under consideration, the significance of the results of the simulation should only be considered semiquantitative. We focus therefore only on systematic trends which are independent of choices in parameters since the latter are not uniquely determined. In view of the arguments given above, parallel-velocity effects and nonlinear effects for dynamical screening potentials are neglected. However, the influence of outer screening on the position of the projectile energy levels ϵ_n has been included through

$$\epsilon_n(R,Q)=-\frac{Q_n^2(R)}{2n^2}+\frac{Q_{\rm eff}(R)-\frac{1}{2}}{4(R-d)}+\sum_{n'=n+1}^{n_{\max}}\frac{P_{n'}(R)}{\langle r\rangle_{n'}}e^{-x}(1+x),\tag{18}$$

with $x=\langle r\rangle_n/\langle r\rangle_{n'}$. The first term represents the hydrogenic energy where the effective charge $Q_n(R)$ includes Slater (inner) screening. The second term describes the image shift

with $Q_{\rm eff}$ denoting the effective charge as seen at the outer fringe of the hollow atom. It includes bound electrons as well as unbound electrons within the radius of the outermost bound shell. The last term represents outer screening [19] from the cloud of the electrons in outer ''shells'' with populations $P_{n'}(R)$. The analytic form of the outer screening function was derived for a $1s$-type orbital with radius $\langle r\rangle_n$. Since for large Q a large number of electrons are transiently bound in outer n shells, outer screening plays a comparatively more prominent role than for multiply charged ions and has therefore been included.

Furthermore, the pileup for charge in outer shells would lead to considerable ''overcharging'' of the projectile. The rate of reionization of quasineutral or slightly negatively charged ions was estimated [5,6] from the average escape time of a free electron moving within kinetic energy $|\epsilon_n|$ (of the order of the Fermi energy) out of the sphere with radius R. For the transient multiply negatively charged hollow atom, $\Delta Q<0$, which can occur for very large Q we estimate the corresponding kinetic energy from the ''Coulomb explosion'' energy $|\Delta Q|/R$. Figure 1 displays the evolution of the charge cloud as a function of R of the hollow atom formed around a Pb^{40+} ion. The dot in the center represents the nucleus and the inner shells $(n=1-4)$. In order to map the classical shell occupation numbers $P_n(R)$ onto a radial charge cloud distribution, we calculated the radial density $\rho(r)$ for hydrogenic wave functions for each n,

$$\rho_A(r)=\sum_{n=1}^{n_{\max}} P(n)\sum_m |\phi_{nlm}(r)|^2. \tag{19}$$

The sum in Eq. (18) extends over all n with negative single-particle binding energy. The choice of $l=l_{\max}$ in Fig. 1 is only intended to clearly display the n-shell structure of the hollow atom. While realistic l distributions are not known it is clear that a more realistic l distribution should weigh more heavily low-l states. Furthermore, these orbitals are strongly perturbed and polarized near the surface (see Refs. [21,22] for more realistic density distributions). For each R, the shell radius $\langle r\rangle_n$ of the most strongly populated shell (darkest countor) is of the order of (or slightly smaller than) the distance of the projectile from the surface. The size of the cloud is an immediate consequence of the over-barrier capture since the distance between the saddle and the projectile must be of the order of the distance from the nucleus to the outer turning point of the hydrogenic orbit. As R decreases the size of the charge cloud shrinks. However, the adjustment is not instantaneous since the depopulation of outer shells occurs with a finite loss rate. Shells with larger radii are rapidly depopulated by reionization into unoccupied state of the solid or into continuum states of the vacuum. One important consequence of the screening cloud forming the hollow atom is the suppression of the further acceleration of the projectile ion towards the surface. The quasineutrality is dynamically maintained by successive capture into lower-n and simultaneous reionization of higher-n shells.

Figure 2 displays the results of our simulation for the energy gain by image acceleration together with recent data for grazing incidence collisions Pb^{Q+} on an Au(110) single-crystal surface ($W=5.38$ eV) with an initial velocity $v_{z,0}\simeq 4.5\times 10^{-3}$ a.u. along the surface normal by Meyer

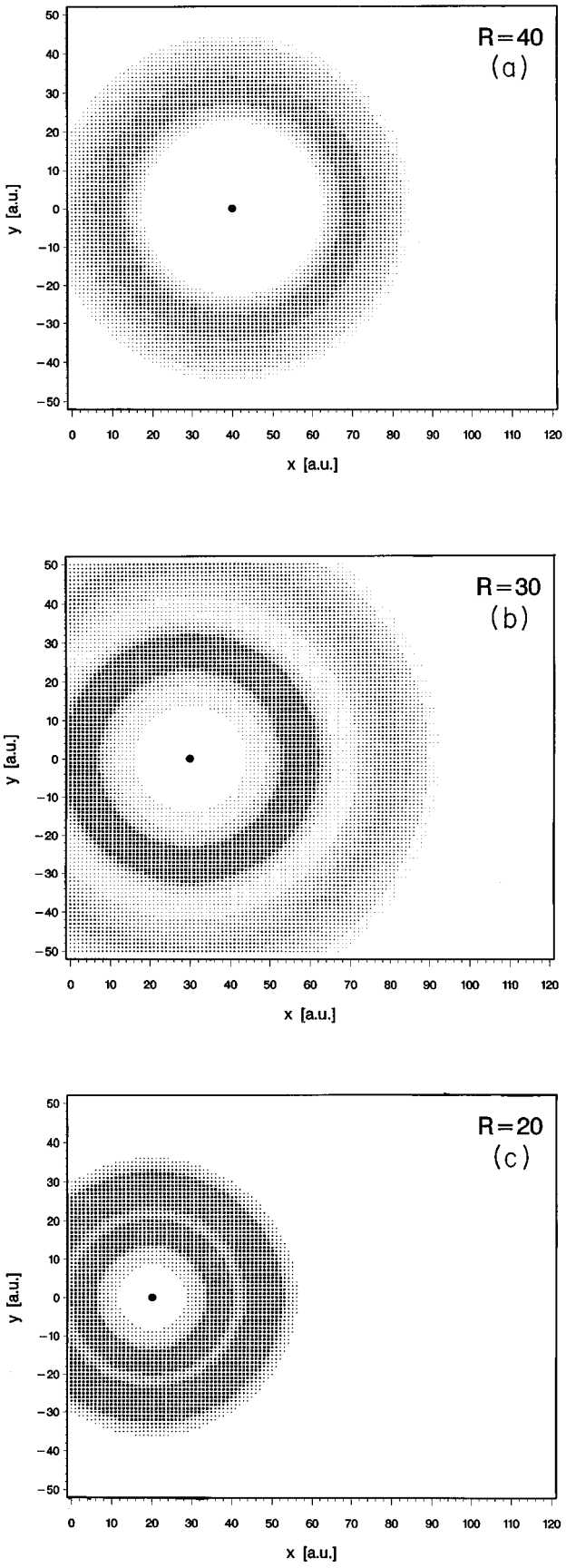

FIG. 1. Evolution of a hollow atom with a Pb^{40+} core in front of Au surface. Note the shrinking radius of the charge cloud. Highest density is at $\langle r\rangle\lesssim R$ as a consequence of the overbarrier condition for capture. Outer ''shells'' get continuously depleted by resonant ionization into the band structure and ionization into the vacuum.

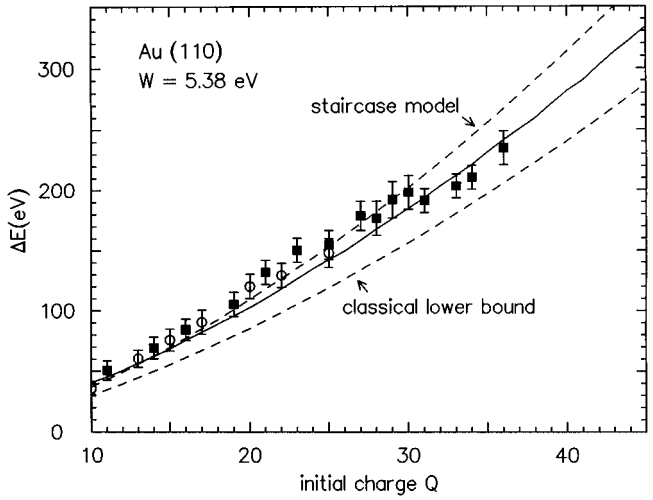

FIG. 2. Energy gain due to image acceleration; ○: I^{q+}; ■: Pb^{q+} from Ref. [3], — simulation. Also shown ar the staircase limit [Eq. (3)], and the classical lower bound [Eq. (20)].

et al. [3]. Also shown are two limiting cases of our simulation: the staircase model [see Eq. (3)] and the classical lower bound for overbarrier neutralization. The latter limit follows from the assumption that the neutralization will be instantaneously complete, i.e., the captured electrons do not slow down subsequent capture due to partial screening as soon as charge transfer becomes classically allowed at R_c. Consequently,

$$\Delta E = \frac{Q^2}{4R_c(Q)} = \frac{W}{4\sqrt{2}} Q^{3/2}. \tag{20}$$

For the staircase curve we use radii $R_c(Q)$ determined from the realistic surface potentials [Eqs. (5) and (6)] rather than the asymptotic image potentials. In agreement with our previous calculations [5] we find that for multiply charged ions with moderate values of Q the simulation yields energy gains exceeding the staircase model. However, for very large Q this trend is reversed: the full simulation falls below the prediction of the staircase model in agreement with recent data [1–3]. We also have observed ''kinks'' and ''plateaus'' in the energy gain at certain charge states. In Fig. 2 weak onsets of plateaus are barely visible near $Q=25$ and near $Q=40$ while in the experiment a more pronounced structure appears near $Q=30$. We note that the position of these structures strongly depends on the choice of parameters for multielectron screening. These variations should therefore be viewed as a measure of the uncertainty of the simulation. The existence of these structures itself is, however, quite general and possesses a simple explanation: for large Q many electrons can be accommodated in the same shell. When one of these shells becomes unbound due to capture into low-lying shells, the hollow atom cannot instantaneously restore quasineutrality. If this ''stripping off'' occurs at a distance R from the surface relatively small compared to $R_c(Q_i)$ but still for $R \gg 1$, the ion experiences an additional image force, resulting in an enhancement of energy gain relative to neighboring charge states.

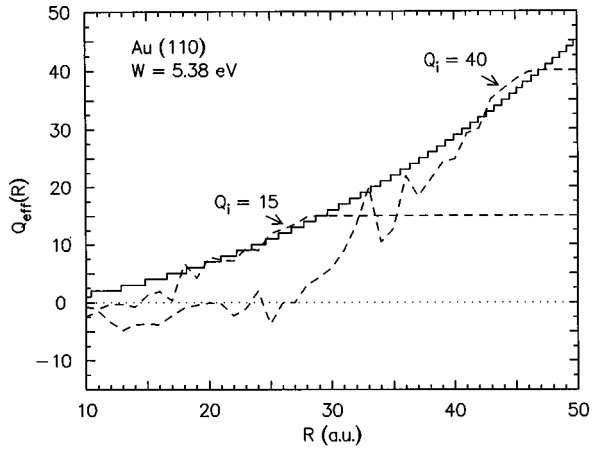

FIG. 3. Evolution of the effective charge state Q_{eff} for Pb^{Q+} with $Q_i=15$ and 40 as a function of R. Also shown is the charge state evolution according to the staircase model. For large Q_i the simulated evolution rapidly deviates from the staircase model.

The—at first glance surprising—crossover as a function of Q of the simulation relative to the staircase model is a consequence of the changes in the neutralization scenario for large Q. Figure 3 illustrates the increasingly strong deviation of the charge state evolution $Q_{\text{eff}}(R)$ from the staircase neutralization. While for $Q_i=15$ the simulated charge state follows the staircase sequence over a considerable fraction ΔR of the total distance $R_c(Q_i)$ between the first capture and the surface, for $Q_i=40$ the charge state very quickly deviates from the staircase and neutralization proceeds faster since the Slater screening of the nucleus by captured electrons is less effective. The simulation lies therefore in between the staircase limit and the classical lower bound. The point of the crossover lies, depending on model parameters, between $Q_i=10$ and $Q_i=20$.

The simple analytic limits [Eqs. (3) and (20)] show an exact linear scaling with W. The simulation obeys this scaling only approximately, since the crossover point as well as

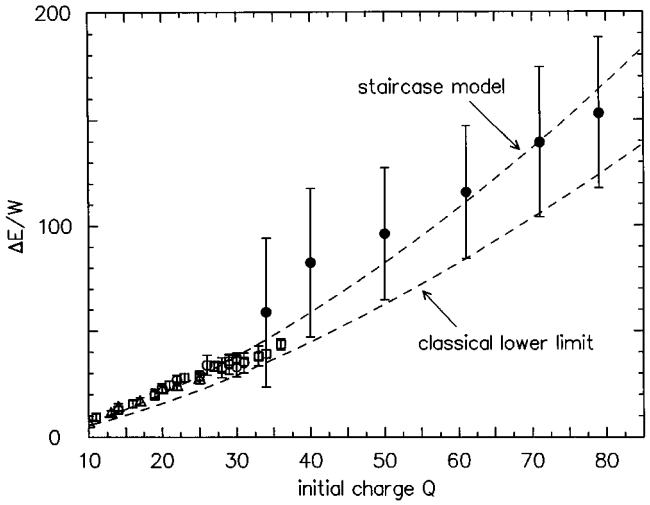

FIG. 4. Scaled energy gain $\Delta E/W$ for different targets. Experimental data: ○: Al [1]; △,□, Au(110) [3]; ●, Au [4]. Also shown are the staircase model [Eq. (3)] and the classical lower bound [Eq. (20)].

the position of the structures are not W independent. Nevertheless, the approximate scaling permits us to compare all experimental data for different targets, Al with $W=4.26$ eV [1,2], polycrystalline Au with $W=5.1$ eV [4], and Au(110) surface with $W=5.38$ eV [3] on a universal plot $\Delta E/W$ (Fig. 4). All data appear to follow the staircase model closely at moderate charge states, but appear to fall below this limit at the very high charge states, in agreement with our simulation.

IV. CONCLUSIONS

We have presented results for the energy gain due to image acceleration of our simulation for above-surface normalization. Unlike previous results for lower charge states, we find for very high charge states energy gains lower than predicted by the simple staircase model. The crossover is due to the fact that for large Q the hollow atom formed along the approach toward the surface can accommodate a large number of electrons due to incomplete Slater screening. Our results reproduce, within the experimental and theoretical uncertainties, available experimental data reasonably well.

ACKNOWLEDGMENTS

This work has been funded by Austrian Fond zur Förderung der wissenschaftlichen Forschung under Project No. P10164-PHY and by the National Science Foundation and by the U.S. Department of Energy, Office of Basic Energy Sciences, Division of Chemical Sciences, under Contract No. DE-AC05-840R21400 with Martin Marietta Energy Systems, Inc.

[1] H. Winter, Europhys. Lett. **18**, 207 (1992).
[2] H. Winter, C. Auth, R. Schuch, and E. Beebe, Phys. Rev. Lett. **71**, 1939 (1993).
[3] F. Meyer, L. Folkerts, H. O. Folkerts, and S. Schippers, Nucl. Instrum. Methods Phys. Res. Sect. B **98**, 441 (1995).
[4] F. Aumayr, H. Kurz, D. Schneider, M. A. Briere, J. McDonald, C. Cunningham, and H. P. Winter, Phys. Rev. Lett. **71**, 1943 (1993).
[5] J. Burgdörfer and F. Meyer, Phys. Rev. A **41**, R20 (1993).
[6] J. Burgdörfer, P. Lerner, and F. Meyer, Phys. Rev. A **44**, 5674 (1991).
[7] C. Setterlind and A. Barany, Nucl. Instrum. Methods Phys. Res. Sect. B **98**, 407 (1995). A misprint in Eq. (14) of Ref. [6], in which $(d/dR)V_p(R,Q(R))$ should read $(1/\mu)(\partial/\partial R)V_p(R,Q(R))$, has apparently misled the authors of this reference to believe that the structures in the charge state evolution $Q_{\rm eff}$ are due to an incorrectly evaluated total derivative. We point out that only properly evaluated partial derivatives enter our calculation. Furthermore, the structures are simply due to the successive stripping off of outer shells, as illustrated in Fig. 1.
[8] P. J. Jennings, R. O. Jones, and M. Weinert, Phys. Rev. B **37**, 6113 (1988); P. J. Jennings and R. O. Jones, Adv. Phys. **37**, 341 (1988).
[9] N. D. Lang and W. Kohn, Phys. Rev. B **1**, 4555 (1970); **3**, 1215 (1971); **7**, 3541 (1973).
[10] F. J. Garcia de Abajo and P. M. Echenique, Phys. Rev. B **46**, 2663 (1992); F. J. Garcia de Abajo, Ph.D. thesis, The University of the Basque Country, San Sebastian, 1993.
[11] R. H. Ritchie and A. L. Marusak, Surf. Sci. **4**, 234 (1966).
[12] P. M. Echenique, R. H. Ritchie, N. Barberan, and J. Inkson, Phys. Rev. B **23**, 6486 (1981).
[13] P. Appell, Nucl. Instrum. Methods Phys. Res. Sect. B **23**, 242 (1987).
[14] H. Schröder and E. Kupfer, Z. Phys. A **279**, 13 (1976); H. Schröder, Nucl. Instrum. Methods Phys. Res. Sect. B **2**, 213 (1984).
[15] J. Los and J. Geerlings, Phys. Rep. **190**, 135 (1990).
[16] H. Winter (unpublished).
[17] R. Köhrbrück, M. Grether, A. Spieler, N. Stolterfoht, R. Page, A. Saal, and J. Bleck-Neuhaus, Phys. Rev. A **50**, 1429 (1994).
[18] F. Meyer, L. Folkerts, and S. Schippers, Nucl. Instrum. Methods Phys. Res. Sect. B **100**, 366 (1995).
[19] J. Burgdörfer, C. Reinhold, and F. Meyer, Nucl. Instrum. Methods Phys. Res. Sect. B **98**, 415 (1995).
[20] R. Diez Muino, A. Arnau, and P. M. Echenique, Nucl. Instrum. Methods Phys. Res. Sect. B **98**, 420 (1995).
[21] S. Deutscher, X. Yang, and J. Burgdörfer, Nucl. Instrum. Methods Phys. Res. Sect. B **100**, 336 (1995); S. Deutscher, X. Yang, J. Burgdörfer, and H. Gabriel (unpublished).
[22] J. Burgdörfer, in *Review of Fundamental Processes and Applications of Atoms and Ions,* edited by C. D. Lin (World Scientific, Singapore, 1993), pp. 517–614.